analytical chemistry

Technical Note

pubs.acs.org/ac

Use of Gel Electrophoresis and Raman Spectroscopy to Characterize the Effect of the Electronic Structure of Single-Walled Carbon Nanotubes on Cellular Uptake

Jennifer L. Chilek,[†] Ruhung Wang,[†,‡] Rockford K. Draper,[†,‡,§] and Paul Pantano*[,†,§]

[†]Department of Chemistry, [‡]Department of Molecular and Cell Biology, and [§]The Alan G. MacDiarmid NanoTech Institute, The University of Texas at Dallas, Richardson, Texas 75080, United States

ABSTRACT: It is well-known that the uptake of single-walled carbon nanotubes (SWNTs) by living cells depends on factors such as SWNT length and surface chemistry. Surprisingly, little is known about whether the electronic structure of a SWNT influences uptake. One reason for this has been the lack of methods to measure the uptake of SWNTs by cell populations. Previously, we developed a rapid, sensitive, and label-free sodium dodecyl sulfate (SDS)-polyacrylamide gel electrophoresis (PAGE) method for measuring the amount of SWNTs in lysates prepared from cultured cells (Wang et al. *Anal. Chem.* **2009**, *81*, 2944). Herein, we describe the use of SDS-PAGE and microprobe Raman spectroscopy to detect and distinguish the electronic structure of SWNTs internalized by mammalian cells. Using normal rat kidney (NRK) cells and SWNTs dispersed with bovine serum albumin (BSA), we demonstrate that the method can detect both metallic and semiconducting SWNTs in lysates of cells that had internalized BSA-SWNTs and that the uptake of BSA-SWNTs by NRK cells is not influenced by SWNT electronic structure.

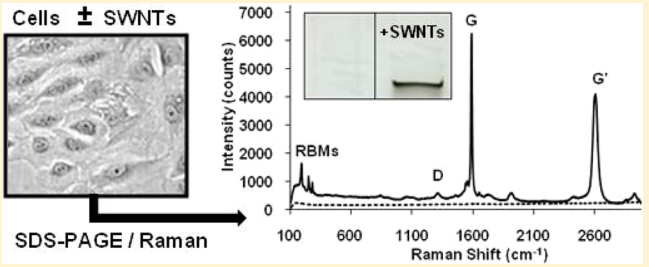

The specific chemical and structural features of carbon nanotubes (CNTs) that may influence their mechanism or rate of uptake by mammalian cells is not well understood.[1,2] For example, two mechanisms have been presented to describe how CNTs enter cells. The first is based on reports that both single-walled CNTs (SWNTs) and multiwalled CNTs (MWNTs) penetrate membranes to appear within the cytoplasm or nucleoplasm of cells.[3−6] Alternatively, there are numerous reports that CNTs enter cells by endocytosis and are found within endosomes and lysosomes of the vacuolar system, segregated from the cytoplasm by a membrane barrier.[7−13] There is also evidence that length affects the uptake of CNTs by cells. For example, studies using DNA-coated CNTs or Pluronic F-127 polymer-coated CNTs have shown that shorter CNTs ($\leq$400 nm) are more readily internalized by mammalian cells.[1,14,15]

One physiochemical property of SWNTs that has not been thoroughly investigated with respect to its influence on cellular uptake is electronic structure. The structural unit of a SWNT is a graphene sheet of sp^2-hybridized carbon atoms rolled into a cylinder, and each SWNT with a unique diameter and chiral angle is distinguished by two rollup vector integers, n and m. Except for very small diameter tubes, SWNT structures for which $n-m$ is evenly divisible by 3 are semimetallic, those for which $n = m$ are metallic, and all others are semiconducting with a band gap that is inversely dependent on the tube diameter.[16] An interesting question is, therefore, whether SWNTs with different electronic structures, and consequently different configurations of carbon atoms on their surfaces, affect their uptake by mammalian cells.

There are several scenarios whereby the electronic structure of a SWNT could influence the uptake process. All start with the foundation that hydrophobic SWNTs are stabilized in water by means of covalent and/or noncovalent functionalization with a dispersant and that uptake is preceded by an interaction with the cell membrane. The first scenario is based on well-known observations that coating SWNTs with certain small-molecule or macromolecular dispersants can encapsulate SWNTs as a function of their electronic structure.[17] It is, therefore, plausible that the electronic structure of exposed SWNT regions could influence how a protein dispersant binds, thereby influencing the protein's secondary structure,[18] which in turn could influence how the protein-coated SWNT interacts with various plasma membrane domains.[19] A second scenario is based on evidence that exposed portions of SWNT sidewalls can trigger nonspecific endocytosis by interaction with hydrophobic domains on the plasma membrane.[20,21] This scenario is supported further by scanning probe microscopy studies of polyethylene glycol (PEG)-coated SWNTs showing that exposed hydrophobic regions of SWNT sidewalls can extend for several tens of nanometers,[20] and pulsed-field gradient NMR studies showing that commonly used pluronic polymer- and albumin protein-dispersants have short-lived

Received: November 25, 2013
Accepted: February 24, 2014
Published: February 24, 2014

   dx.doi.org/10.1021/ac403827m | *Anal. Chem.* 2014, 86, 2882−2887

(≤50 ms) residence times on SWNT surfaces.[22,23] It is, therefore, plausible that the surface of any covalently or noncovalently functionalized SWNT may not be completely covered by dispersant at any given time, and thus, the electronic structure of a SWNT could influence how it interacts with a cell membrane through transiently exposed hydrophobic surface regions, even in the presence of dispersants.

Progress in understanding the physiochemical properties of SWNTs that influence their cellular uptake is also hampered by the difficulty in detecting cell-associated SWNTs (i.e., SWNTs bound to and/or internalized by cells) from a population of cells. This not the case for nanoparticles comprising or containing metals since their cell-associated levels can be easily detected above the high background of carbon in a biological matrix using inductively coupled plasma mass spectroscopy (ICPMS). In contrast, the most common methods to detect cell-associated SWNTs, namely, electron, ultraviolet/visible fluorescence, near-infrared photoluminescence, and Raman microscopies, are all high spatial resolution techniques whose use is impractical in generating an average measure of cell populations for statistical analysis of experimental variability.[24] In response to this analytical challenge, we previously developed a rapid, sensitive, and label-free sodium dodecyl sulfate (SDS)-polyacrylamide gel electrophoresis (PAGE) method for measuring the amount of SWNT material in lysate samples prepared from a large number of cultured cells;[25] and recently, we demonstrated the usefulness of the method in guiding the accurate assessment of a comparative SWNT cytotoxicity analysis.[12]

Herein, we demonstrate the use of SDS-PAGE and microprobe Raman spectroscopy to assess whether the electronic structure of a SWNT influences the cell uptake process. Using normal rat kidney (NRK) cells and SWNTs dispersed with bovine serum albumin (BSA), we first demonstrate that the SDS-PAGE/Raman method can detect and distinguish metallic and semiconducting SWNTs present in dispersed BSA-SWNT samples and lysate samples of cells that had taken-up SWNTs. Next, we demonstrate that the ratio of the most abundant metallic and semiconducting SWNT structures identified in the Raman spectra of lysate samples of SWNT-treated cells is identical to the ratio observed for the BSA-SWNT dispersions applied to cells, suggesting that the electronic structure of SWNTs coated with BSA does not influence SWNT uptake by NRK cells.

EXPERIMENTAL SECTION

Chemicals and Solutions. Raw HiPco SWNT powder (lot no. R0559; ∼75 w % carbonaceous and ∼22 w % metallic species as determined by TGA) was purchased from Unidym Inc.; caution, a particulates respirator should be worn when handling dry SWNT powders. Dulbecco's modified Eagle medium (DMEM) was purchased from Irvine Scientific and was supplemented with 37 mg/mL sodium bicarbonate, 4.5 mg/mL D-glucose, 0.29 mg/mL L-glutamine, 10 mM HEPES, 15 mg/L phenol red, 100 units/mL penicillin, 0.1 mg/mL streptomycin, and 2.5 μg/mL amphotericin B. DMEM further supplemented with 5% (v/v) fetal bovine serum (FBS; HyClone) is denoted DMEM/FBS. Phosphate buffered saline (PBS; 8 mM phosphate, 150 mM NaCl, pH 7.4) was sterilized by autoclaving at 120 °C for 0.5 h. Deionized water (18.2 MΩ cm) was obtained using a Barnstead Nanopure Infinity water purification system. BSA solutions were prepared by dissolving 10 g of BSA in 100 mL of sterile deionized water, adjusting the pH to 7.4, and filtering the solution through a 0.22-μm pore membrane. All other chemicals were purchased from Sigma-Aldrich unless otherwise noted.

Preparation of BSA-SWNT Dispersions. A sonication/centrifugation protocol was used to process dry SWNT powders into aqueous BSA-SWNT dispersions. Specifically, 1.0 mg of HiPco SWNT powder was mixed with 1.0 mL of BSA solution in a 1.5-mL Eppendorf tube and then probe sonicated at 0 °C. Probe sonication was performed using a Branson 250 Sonifier operated at 10 W with the ice-cooled, 3-mm diameter probe tip centered 5 mm from the bottom of the tube. After 10 min of sonication, the resulting black suspension was centrifuged in an Eppendorf 5424 centrifuge for 8 min at 21 000*g*. The upper ∼900 μL of the supernatant was recovered without disturbing the sediment and placed in a clean microcentrifuge tube before a second 8-min centrifugation at 21 000*g* was performed. The upper ∼850 μL of the second supernatant was recovered, and this process was repeated with 21 000*g* centrifugation with times of 16 and 42 min to yield a third and fourth supernatant, respectively. BSA-SWNT dispersions could be stored at 4 °C for at least 1 month without any SWNTs precipitating out of solution.

Characterization of BSA-SWNT Dispersions. The amount of HiPco-SWNT material (i.e., SWNTs and related carbonaceous species) in BSA-SWNT dispersions was ∼75 μg/mL as determined using the SDS-PAGE method.[12,25] In brief, 1.0 mg of as-received HiPco powder was sonicated in 1.0 mL of 100 mg/mL BSA solution to generate a standard dispersion that did not involve selective removal of material by centrifugation. The standard dispersion was loaded in increasing volumes in separate lanes and electrophoresed at 100 V for 2 h. Following electrophoresis, a digitized gel image was acquired and a calibration curve was constructed using the quantified pixel intensities of the SWNT-containing bands that were corrected by the weight percentage of carbon species (75%) in the powder. The pixel intensity acquired from a gel band of a known volume of a BSA-SWNT dispersion loaded in the gel was then used to estimate the amount of HiPco-SWNT material in the BSA-SWNT dispersion. Absorption spectra of BSA-SWNT dispersions were acquired using a dual-beam Perkin-Elmer Lambda 900 UV−vis-NIR spectrophotometer with a scan speed of 125.00 nm/min and integration times of 0.48 s. All spectra were background corrected against a sonicated/centrifuged BSA control solution. The total metals detected in the fourth supernatant (also known as a BSA-SWNT dispersion) was <2 ppm as determined by ICPMS.[25]

Cell Culture. Normal rat kidney (NRK) cells were obtained from the American Type Culture Collection and were cultured in DMEM/FBS in a 37 °C incubator with 90% air and 10% CO_2. To determine the number of cells in a given dish, the cells were detached using 0.05% (w/v) trypsin-EDTA. Aliquots of these cell suspensions were diluted in Isoton-II isotonic solution, and the number of cells was measured using a Beckman Coulter Z1 particle counter. SWNT uptake experiments involved inoculating 1×10^6 cells in 100-mm tissue culture dishes in DMEM/FBS. The cells were incubated at 37 °C for 24 h to allow them to adhere to the bottom of dishes. After the initial 24-h incubation, the cells were washed twice with PBS before the addition of either fresh control media, prepared by mixing 2×-concentrated DMEM/FBS in a 1:1 ratio with water or experimental media, prepared by mixing 2×-concentrated DMEM/FBS in a 1:1 ratio with a BSA-SWNT dispersion containing ∼75 μg/mL of HiPco-SWNT material.

dx.doi.org/10.1021/ac403827m | Anal. Chem. 2014, 86, 2882−2887

This resulted in a concentration of ~38 μg/mL of HiPco-SWNT material in medium that was added to the cells, which were then incubated at 37 °C for 3 days.

Extracting SWNTs from Cells. Following the 3-day incubation, cells were washed twice with DMEM/FBS and twice with PBS before being detached from the dish with trypsin. The suspended cells were collected by gentle centrifugation at 60*g* for 7 min, resuspended in PBS to remove traces of trypsin and centrifuged again. Cells in the pellet were lysed by suspending them in a 200-μL mixture of 1% SDS, 1 mM $MgCl_2$, and 1 mM $CaCl_2$ for 2 h at 37 °C. The cell lysate were then treated with 20 μg of DNase I for 2 h at 37 °C to degrade released DNA and reduce the solution viscosity.

SDS-PAGE of Cell Lysates. SDS-PAGE of cell lysate samples was performed using a standard Hoefer Mini Vertical Gel as described previously by Wang et al.[25] Lysate samples (60 μL prepared from control or SWNT-treated cells) were loaded in separate lanes and electrophoresed at 100 V for 2 h before each lane was analyzed by microprobe Raman spectroscopy.

Raman Spectroscopy. All Raman spectra were acquired using a Horiba Jobin Yvon high-resolution LabRam HR800 Raman spectrometer with a 450-μm entrance slit and an 1100-μm confocal pinhole. Wavenumber calibration was performed using the 520.5 cm^{-1} line of a silicon wafer, and the spectral resolution was ~5 cm^{-1}. The 632.8-nm laser excitation was provided by a Spectra-Physics model 127 helium−neon laser operating at 20 mW. The typical power delivered to the sample was 3 mW as measured using a Newport model-1815C power meter with an 818UV series photodetector. Raman spectra of aqueous BSA-SWNT dispersions (500-μL samples dispensed into 35-mm glass-bottom imaging dishes (MatTek)) were acquired using a 50×/0.5 NA LM-Plan objective. Raman spectra of SDS-PAGE bands (obtained by removing ~4 mm^2 of material around a gel band and placing it flat on an imaging dish) were acquired using a 100×/0.9 NA M-Plan objective. Raman spectra between 100 and 3000 cm^{-1} were acquired with 5-s integration times and were plotted as the average of three spectra, and spectra between 150 and 350 cm^{-1} were acquired with 10-s integration times and were plotted as the average of 10 spectra. All peak positions were obtained by Lorentzian fitting of the corresponding spectral region as described by Strano et al.[26]

RESULTS AND DISCUSSION

Characterization of BSA-SWNT Dispersions. HiPco SWNTs were chosen for this work because they characteristically contain a variety of metallic and semiconducting SWNT structures that are amenable to resonant Raman spectroscopic analysis using 632.8-nm laser excitation. The biocompatible dispersant chosen for this work was BSA, a water-soluble protein well-known to noncovalently coat pristine SWNTs.[10,12,27−30] All BSA-SWNT dispersions were prepared using a sonication and centrifugation protocol adapted from Smalley and co-workers.[31] The first advantage of this protocol is the effective removal of heavier metal-containing SWNTs and bundles (e.g., >99% of the metals present in the HiPco SWNT powder were not detected by ICPMS in BSA-SWNT dispersions).[25,32] Another advantage is the facile production of individually dispersed SWNTs and small bundles with short (<500 nm) lengths as determined using scanning probe microscopy.[12,33] UV−vis-NIR spectroscopy was also used to characterize BSA-SWNT dispersions since the observation of sharp van Hove peaks is indicative of aqueous solutions containing individually dispersed SWNTs.[28] Figure 1,top shows a representative absorption spectrum of a BSA-SWNT

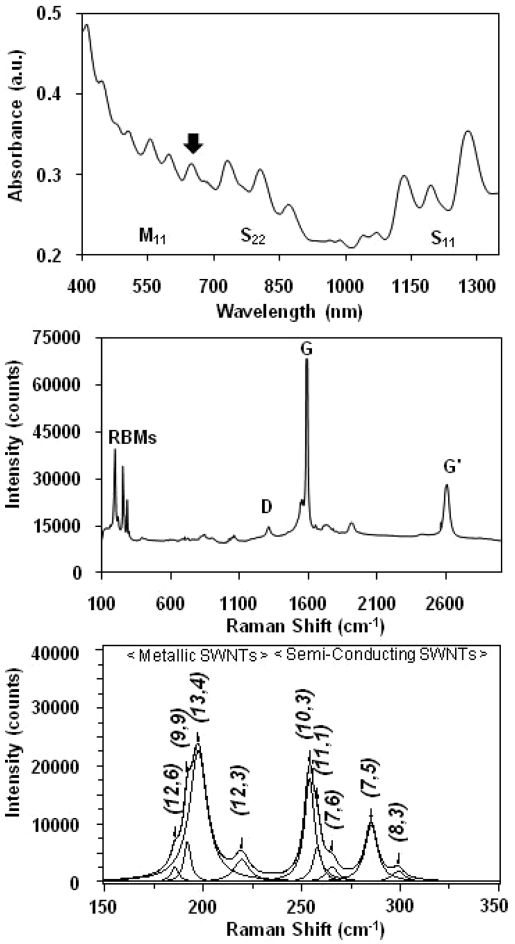

Figure 1. (Top) Representative background-corrected UV−vis-NIR absorption spectrum of a HiPco BSA-SWNT dispersion; the arrow denotes ~630 nm. (Middle) Representative Raman spectrum (632.8-nm laser excitation) of a HiPco BSA-SWNT dispersion showing the radial breathing modes (RBMs), the D-band, the G-band, and the G′-band. (Bottom) Representative baseline-corrected 632.8-nm Raman spectrum of a HiPco BSA-SWNT dispersion where the peak positions of the four metallic and five semiconducting SWNT structures (denoted by their (*n*,*m*) chiral indices) were obtained by curve fitting of the RBM region using a summation of Lorentzian line shapes.

dispersion prepared using four rounds of centrifugation where the sharp absorption features correspond to the M_{11}, S_{22}, and S_{11} optical transitions of the metallic and semiconducting SWNT structures contained in these dispersions. Of particular interest is the spectral feature observed at ~630 nm which appears to be a combination of several overlapping peaks, most likely the M_{11} transition of metallic (13,4) SWNT structures which absorb at ~626 nm, and the S_{22} transition of semiconducting (10,3) SWNT structures which absorb at ~633 nm.[16]

Raman spectroscopy was used to characterize dispersed SWNT samples, and the diameter dependence of the radial breathing modes (RBMs) was used to identify the particular SWNT structures that are resonant with 632.8-nm excitation.[34,35] Figure 1,middle shows a representative Raman spectrum of a BSA-SWNT dispersion acquired with 632.8-nm excitation energy, chosen because it probes metallic tubes with

dx.doi.org/10.1021/ac403827m | *Anal. Chem.* 2014, 86, 2882−2887

diameters >1.1 nm and semiconducting tubes with diameters <1.1 nm.[36] The spectrum shows a number of well-characterized SWNT resonances, such as RBMs in the 150−350-cm^{-1} region, the disorder-induced mode (D-band) at ∼1280 cm^{-1}, the tangential stretching mode (G-band) at ∼1585 cm^{-1}, and the second-order G′-band at ∼2595 cm^{-1}.[37−39] Figure 1,bottom shows an expanded view of the RBM spectral region where two distinct bands are observed, a low-frequency group of peaks between 175 and 225 cm^{-1} and a high-frequency group between 225 and 300 cm^{-1}.

Since it is well-known that the RBM spectral features of SWNTs are sensitive to bundling, a series of Raman analyses described by Hennrich et al.[36] were performed to ensure that our structural assignments would not be affected by the aggregation state of BSA-SWNTs prepared using four rounds of centrifugation. These analyses involved the use of a bundling ratio featuring (12,3) SWNTs since these structures are in-resonance with ∼560-nm excitation when individually dispersed but resonate at higher wavelengths (e.g., ∼633 nm) when bundled.[26,36] As shown in Figure 2, the (12,3)/(13,4)-bundling ratio (i.e., the ratio of the peak area of the (12,3) resonance at ∼219 cm^{-1} to the peak area of the (13,4) resonance at ∼197 cm^{-1}) calculated for the spectrum acquired from BSA-SWNTs prepared using four rounds of centrifugation was 0.17. For comparison, the (12,3)/(13,4)-bundling ratio calculated for a heavily bundled reference sample (i.e., the first sediment of the BSA-SWNT dispersion-making process) was 1.22 and that for BSA-SWNTs acquired from the third supernatant of the process was 0.30 (Figure 2). Since additional centrifugation steps did not improve upon the 0.17-bundling ratio, all remaining experiments involved well-dispersed BSA-SWNTs obtained from the fourth supernatant of the dispersion-making process.

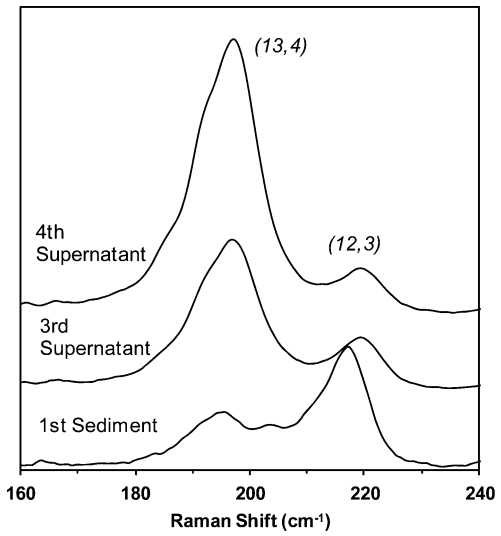

Figure 2. Representative baseline-corrected Raman spectra (632.8-nm laser excitation) of a HiPco BSA-SWNT dispersion (i.e., the fourth supernatant), the third-supernatant of the BSA-SWNT dispersion protocol, and the sediment from the first centrifugation of the BSA-SWNT dispersion protocol; the (12,3)/(13,4) bundling ratios of the three samples were 0.17, 0.30, and 1.22, respectively. The spectra were offset for clarity and normalized to a common intensity scale.

Assignment of RBM peak frequencies to specific (*n*,*m*) SWNT structures present in BSA-SWNT dispersions was performed according to the methods of Strano et al.[26] As shown in Figure 1,bottom, the predominant SWNT identified in the low-frequency RBM region was a metallic (13,4) structure with a 1.22-nm diameter and the predominant SWNT identified in the high-frequency RBM region was a semiconducting (10,3) structure with a 0.92-nm diameter. Other metallic SWNTs identified in the low-frequency RBM region were (12,6), (9,9), and (12,3) structures, and other semiconducting SWNTs identified in the high-frequency RBM region were (11,1), (7,6), (7,5), and (8,3) structures. As shown in Table 1, there is considerable agreement between these assignments and those observed by others using HiPco SWNTs. Specifically, the RBM frequencies of the four metallic structures observed in BSA-SWNT dispersions were within 2% of those reported by Strano et al. for SDS-dispersed HiPco SWNT samples,[26] and the RBM frequencies of the five semiconducting structures observed in BSA-SWNT dispersions were within 1% of those reported by Hennrich et al. for sodium dodecylbenzenesulfonate (SDBS)-dispersed HiPco SWNT samples.[36] In summary, this Raman data demonstrates that the metallic and semiconducting SWNT resonances in HiPco BSA-SWNT dispersions are clearly distinguishable when probed with 632.8-nm excitation energy, in accordance with previous reports.[26,40]

SDS-PAGE/Raman Analyses of SWNT Material Extracted from NRK Cells. The SDS-PAGE method exploits the observation that when aqueous SWNT-containing samples are added to a SDS solution and then subjected to SDS-PAGE, the SWNT material accumulates in a single band at the interface between the loading well and the stacking gel, and not elsewhere on the gel (Figure 3,inset). In our previous work, the detection of cell-associated SWNT material was demonstrated by incubating NRK cells in medium containing BSA-SWNTs at

Table 1. Proposed (*n*,*m*) Assignments for the Metallic and Semi-Conducting RBM Frequencies Observed in the Spectra of HiPco BSA-SWNT Dispersions (Figure 1,Bottom)

metallic SWNT resonances (low-frequency RBM region)				semi-conducting SWNT resonances (high-frequency RBM region)			
(*n*,*m*) assignment	observed ω_{RBM} (cm^{-1})	reported[a] ω_{RBM} (cm^{-1})	diameter (nm)	(*n*,*m*) assignment	observed ω_{RBM} (cm^{-1})	reported[b] ω_{RBM} (cm^{-1})	diameter (nm)
(12,6)	186	190	1.26	(10,3)	254	254	0.92
(9,9)	192	193	1.24	(11,1)	258	258	0.90
(13,4)	197	195	1.22	(7,6)	266	266	0.88
(12,3)	219	217	1.09	(7,5)	285	284	0.82
				(8,3)	299	301	0.77

[a]Assignments for the metallic RBM frequencies of HiPco SDS-SWNT dispersions reported by Strano et al.[26] [b]Assignments for the semiconducting RBM frequencies of HiPco SDBS-SWNT dispersions reported by Hennrich et al.[36]

dx.doi.org/10.1021/ac403827m | Anal. Chem. 2014, 86, 2882−2887

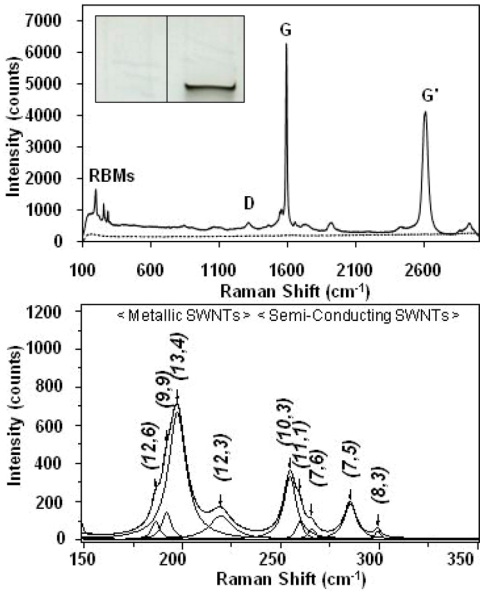

Figure 3. (Inset) Representative image of an 11 mm × 6 mm region of a SDS-PAGE gel showing the control (left) and sample (right) lanes. (Top) Representative Raman spectra (632.8-nm laser excitation) acquired from a SDS-PAGE gel lane loaded with lysate from cells incubated in medium containing ~38 μg/mL HiPco BSA-SWNT material (solid line), and a control gel lane loaded with lysate from NRK cells incubated in medium without SWNTs (dashed line), following electrophoresis at 100 V for 2 h. (Bottom) Representative baseline-corrected 632.8-nm Raman spectrum of the RBM region acquired from the dark band in a SDS-PAGE gel lane loaded with lysate from cells incubated in medium containing ~38 μg/mL HiPco BSA-SWNT material following electrophoresis at 100 V for 2 h. The peak positions of the four metallic and five semiconducting SWNT structures (denoted by their (n,m) chiral indices) were obtained by curve fitting of the RBM region using a summation of Lorentzian line shapes.

various temperatures for 1−3 days.[25] After incubation, the cells were washed and lysed, and cell-associated SWNT material was extracted from the lysate and quantified using SDS-PAGE. Using this method, the uptake of SWNT material by NRK cells was observed to be linear with time and the applied dose and was not observed at low temperatures, which is consistent with an uptake model involving fluid-phase endocytosis.

The same SWNT uptake and extraction protocols were followed in the present work with NRK cells that were incubated with BSA-SWNT dispersions at 37 °C for 3 d. Aliquots of lysates from cells incubated in medium containing ~38 μg/mL of BSA-SWNT material (and from control cells incubated in medium that did not contain BSA-SWNTs) were subjected to SDS-PAGE at 100 V for 2 h, and dark bands of material were evident only at the loading well/stacking gel interface of lanes loaded with lysate from SWNT-treated cells. Figure 3,top shows a representative Raman spectrum acquired from the interface of the control gel lane, which demonstrates that there are no Raman peaks emanating from control cells or the PA gel that would interfere with the analysis of SWNT signals. Figure 3,top also shows a representative Raman spectrum acquired from the dark band of material observed in the gel lane that contained lysate from SWNT-treated cells; this spectrum displays all of the well-characterized SWNT resonances observed in the spectrum of the dispersed SWNT sample (Figure 1,middle).

Raman spectroscopy was also used to determine if the same metallic and semiconducting SWNTs identified in aqueous BSA-SWNT dispersions would be observed in the SWNT-containing gel bands of cell lysate samples. As shown in Figure 3,bottom, the same nine peaks observed in the low-frequency and high-frequency RBM bands in the spectrum of BSA-SWNT dispersions are detected in the spectrum acquired from the lysate of SWNT-treated cells. In addition, it is important to note that the (12,3)/(13,4) bundling ratio acquired from the gel bands of SWNT-treated cell lysates was determined to be 0.24, which suggests that this material is not heavily bundled and would therefore not influence SWNT structural assignments. In fact, the RBM frequencies of the four metallic and five semiconducting SWNT resonances acquired from SWNT-containing gel bands were within 1% of those observed for BSA-SWNT dispersions (Table 1). In summary, since all the SWNT structures identified in the Raman spectrum of BSA-SWNT dispersions applied to cells (Figure 1) were observed in the Raman spectrum acquired from the dark gel bands of SWNT material extracted from cells (Figure 3), these results demonstrate that the SDS-PAGE/Raman method can detect and distinguish metallic and semiconducting SWNT structures in lysates of cells that had taken-up BSA-SWNTs. Furthermore, the similar aggregation states of SWNTs observed in aqueous dispersions and gel bands permits an assessment of preferential uptake of metallic or semiconducting SWNTs through a comparison of RBM peak areas of BSA-SWNT dispersions and lysate samples of SWNT-treated cells, as described next.

Does the Uptake of BSA-SWNTs Depend on the Electronic Structure of the SWNTs? To assess whether the electronic structure of BSA-coated SWNTs plays a role in the NRK cell uptake process, the metallic and semiconducting SWNTs observed in BSA-SWNT dispersions were compared to those observed in lysate samples of SWNT-treated cells. Specifically, the ratio of the Lorentzian areas of the predominant SWNT structures observed in the low- and high-frequency RBM regions (i.e., metallic (13,4) SWNTs and semiconducting (10,3) SWNTs, respectively) was determined using spectra acquired from BSA-SWNT dispersions and lysate samples of SWNT-treated cells. For BSA-SWNT dispersions, the mean (13,4)/(10,3) ratio was 2.3 ± 0.12 (n = 6 spectra from n = 6 dispersions) and for SWNT-containing cell lysates, the ratio was 2.4 ± 0.44 (n = 6 spectra from n = 3 gels). Since the ratios for BSA-SWNT dispersions and SWNT-containing lysates are nearly identical, the electronic structure of a BSA-SWNT does not appear to influence the uptake of SWNTs by NRK cells. This finding is supported by our previous work where the uptake of BSA-SWNT material was shown to be consistent with a fluid-phase endocytosis model.[25] With this model, as long as a particle is small enough, the particle and the surrounding fluid are engulfed and internalized in a vesicle/endosome regardless of the chirality of the SWNT. Conversely, if SWNTs were to penetrate cells by passive diffusion or enter cells by a selective uptake mechanism that involved a direct interaction between the cell membrane and exposed SWNT regions, an electronic-structure dependence would be possible that could favor certain SWNT structures. Of course, one should not rule out the possibility that the behavior observed here with HiPco-SWNT material will be different with other mammalian cell lines and SWNT products.

dx.doi.org/10.1021/ac403827m | Anal. Chem. 2014, 86, 2882−2887

CONCLUSION

The key attributes of the SDS-PAGE method are that it enables a population of cells to be assayed for cell-associated SWNT material, and it enables straightforward investigations of SWNT parameters involved in the uptake process (e.g., SWNT lengths, concentrations, and surface chemistries), as well as, parameters required to assess the energy dependence of uptake (e.g., cell incubation times and temperatures).[12,25] Herein, we demonstrated that SDS-PAGE/Raman spectroscopy can detect and distinguish metallic and semiconducting SWNTs in lysate samples of cells that had taken-up SWNT material and that the uptake of BSA-coated SWNTs by NRK cells is not influenced by the electronic structure of the SWNTs. Since an enhanced understanding of the fundamental interactions between cells and various SWNT structures is required for a number of biomedical applications, we anticipate that the SDS-PAGE/Raman method should find use in identifying metallic and semiconducting SWNT structures in a variety of samples.

AUTHOR INFORMATION

Corresponding Author

*E-mail: pantano@utdallas.edu.

Notes

The authors declare no competing financial interest.

ACKNOWLEDGMENTS

The authors thank the SEMATECH/Semiconductor Research Corporation (Grant ERC 425-042), the National Institutes of Health AREA Program (Grant R15-CA152917-01A1), and the Robert A. Welch Foundation for supporting this work and Nancy S. Jacobsen for her scientific contributions to this work.

REFERENCES

(1) Raffa, V.; Ciofani, G.; Nitodas, S.; Karachalios, T.; D'Alessandro, D.; Masini, M.; Cuschieri, A. *Carbon* **2008**, *46*, 1600−1610.
(2) Iversen, T.-G.; Skotland, T.; Sandvig, K. *Nano Today* **2011**, *6*, 176−185.
(3) Pantarotto, D.; Briand, J.-P.; Prato, M.; Bianco, A. *Chem. Commun.* **2004**, 16−17.
(4) Bianco, A.; Kostarelos, K.; Partidos, C. D.; Prato, M. *Chem. Commun.* **2005**, 571−577.
(5) Kostarelos, K.; Lacerda, L.; Pastorin, G.; Wu, W.; Wieckowski, S.; Luangsivilay, J.; Godefroy, S.; Pantarotto, D.; Briand, J.-P.; Muller, S.; Prato, M.; Bianco, A. *Nat. Nanotechnol.* **2007**, *2*, 108−113.
(6) Lacerda, L.; Russier, J.; Pastorin, G.; Herrero, M. A.; Venturelli, E.; Dumortier, H.; Al-Jamal, K. T.; Prato, M.; Kostarelos, K.; Bianco, A. *Biomaterials* **2012**, *33*, 3334−3343.
(7) Shi Kam, N. W.; Jessop, T. C.; Wender, P. A.; Dai, H. *J. Am. Chem. Soc.* **2004**, *126*, 6850−6851.
(8) Jin, H.; Heller, D. A.; Strano, M. S. *Nano Lett.* **2008**, *8*, 1577−1585.
(9) Cherukuri, P.; Bachilo, S. M.; Litovsky, S. H.; Weisman, R. B. *J. Am. Chem. Soc.* **2004**, *126*, 15638−15639.
(10) Shi Kam, N. W.; Dai, H. *J. Am. Chem. Soc.* **2005**, *127*, 6021−6026.
(11) Marches, R.; Mikoryak, C.; Wang, R. H.; Pantano, P.; Draper, R. K.; Vitetta, E. S. *Nanotechnology* **2011**, *22*, 095101 (10 pp).
(12) Wang, R.; Mikoryak, C.; Li, S.; Bushdiecker, D., II; Musselman, I. H.; Pantano, P.; Draper, R. K. *Mol. Pharmaceutics* **2011**, *8*, 1351−1361.
(13) Lamprecht, C.; Gierlinger, N.; Heister, E.; Unterauer, B.; Plochberger, B.; Brameshuber, M.; Hinterdorfer, P.; Hild, S.; Ebner, A. *J. Phys.: Condens. Matter* **2012**, *24*, 164206 (9pp).
(14) Jin, H.; Heller, D. A.; Sharma, R.; Strano, M. S. *ACS Nano* **2009**, *3*, 149−158.
(15) Becker, M. L.; Fagan, J. A.; Gallant, N. D.; Bauer, B. J.; Bajpai, V.; Hobbie, E. K.; Lacerda, S. H.; Migler, K. B.; Jakuadma, J. P. *Adv. Mater.* **2007**, *19*, 939−945.
(16) Weisman, R. B.; Bachilo, S. M. *Nano Lett.* **2003**, *3*, 1235−1238.
(17) Hersam, M. C. *Nat. Nanotechnol.* **2008**, *3*, 387−394.
(18) Karajanagi, S. S.; Vertegel, A. A.; Kane, R. S.; Dordick, J. S. *Langmuir* **2004**, *20*, 11594−11599.
(19) Popescu, B. M.; Ali, N.; Basturea, G.; Comsa, G. I.; Materon, L. A.; Chipara, M. *Appl. Surf. Sci.* **2013**, *275*, 2−6.
(20) Delogu, L. G.; Stanford, S. M.; Santelli, E.; Magrini, A.; Bergamaschi, A.; Motamedchaboki, K.; Rosato, N.; Mustelin, T.; Bottini, N.; Bottini, M. *J. Nanosci. Nanotechnol.* **2010**, *10*, 5293−5301.
(21) Bottini, M.; Rosato, N.; Bottini, N. *Biomacromolecules* **2011**, *12*, 3381−3393.
(22) Frise, A. E.; Pagès, G.; Shtein, M.; Pri Bar, I.; Regev, O.; Furó, I. *J. Phys. Chem. B* **2012**, *116*, 2635−2642.
(23) Frise, A. E.; Edri, E.; Furó, I.; Regev, O. *J. Phys. Chem. Lett.* **2010**, *1*, 1414−1419.
(24) Pantano, P.; Draper, R. K.; Mikoryak, C.; Wang, R. Electrophoretic methods to quantify carbon nanotubes in biological cells. In *Handbook of Carbon Nano Materials*; D'Souza, F., , Kadish, K. M., Eds.; World Scientific Publishers: Singapore, 2012; Vol. *3*, pp 83−106.
(25) Wang, R.; Mikoryak, C.; Chen, E.; Li, S.; Pantano, P.; Draper, R. K. *Anal. Chem.* **2009**, *81*, 2944−2952.
(26) Strano, M. S.; Doorn, S. K.; Haroz, E. H.; Kittrell, C.; Hauge, R. H.; Smalley, R. E. *Nano Lett.* **2003**, *3*, 1091−1096.
(27) Edri, E.; Regev, O. *Anal. Chem.* **2008**, *80*, 4049−4054.
(28) Karajanagi, S. S.; Yang, H.; Asuri, P.; Sellitto, E.; Dordick, J. S.; Kane, R. S. *Langmuir* **2006**, *22*, 1392−1395.
(29) Matsuura, K.; Saito, T.; Okazaki, T.; Ohshima, S.; Yumura, M.; Iijima, S. *Chem. Phys. Lett.* **2006**, *429*, 497−502.
(30) Elgrabli, D.; Abella-Gallart, S.; Aguerre-Chariol, O.; Robidel, F.; Rogerieux, F.; Boczkowski, J.; Lacroix, G. *Nanotoxicology* **2007**, *1*, 266−278.
(31) O'Connell, M. J.; Bachilo, S. M.; Huffman, C. B.; Moore, V. C.; Strano, M. S.; Haroz, E. H.; Rialon, K. L.; Boul, P. J.; Noon, W. H.; Kittrell, C.; Ma, J.; Hauge, R. H.; Weisman, R. B.; Smalley, R. E. *Science* **2002**, *297*, 593−596.
(32) Yehia, H. N.; Draper, R. K.; Mikoryak, C.; Walker, E. K.; Bajaj, P.; Musselman, I. H.; Daigrepont, M. C.; Dieckmann, G. R.; Pantano, P. *J. Nanobiotechnol.* **2007**, *5*, 8−24.
(33) Chin, S.-F.; Baughman, R. H.; Dalton, A. B.; Dieckmann, G. R.; Draper, R. K.; Mikoryak, C.; Musselman, I. H.; Poenitzsch, V. Z.; Xie, H.; Pantano, P. *Exp. Biol. Med.* **2007**, *232*, 1236−1244.
(34) Heller, D. A.; Barone, P. W.; Swanson, J. P.; Mayrhofer, R. M.; Strano, M. S. *J. Phys. Chem. B* **2004**, *108*, 6905−6909.
(35) Fantini, C.; Jorio, A.; Souza, M.; Strano, M. S.; Dresselhaus, M. S.; Pimenta, M. A. *Phys. Rev. Lett.* **2004**, *93* (147406), 1−4.
(36) Hennrich, F.; Krupke, R.; Lebedkin, S.; Arnold, K.; Fischer, R.; Resasco, D. E.; Kappes, M. M. *J. Phys. Chem. B* **2005**, *109*, 10567−10573.
(37) Resasco, D. E.; Herrera, J. E. *Encyclopedia Nanosci. Nanotechnol.* **2004**, *10*, 125−147.
(38) Dresselhaus, M. S.; Dresselhaus, G.; Jorio, A.; Souza Filho, A. G.; Saito, R. *Carbon* **2002**, *40*, 2043−2061.
(39) Pimenta, M. A.; Marucci, A.; Empedocles, S. A.; Bawendi, M. G.; Hanlon, E. B.; Rao, A. M.; Eklund, P. C.; Smalley, R. E.; Dresselhaus, G.; Dresselhaus, M. S. *Phys. Rev. B: Condens. Matter Mater. Phys.* **1998**, *58*, R16016−R16019.
(40) Krupke, R.; Hennrich, F.; Löhneysen, H. v.; Kappes, M. M. *Science* **2003**, *301*, 344−347.